J Neuropathol Exp Neurol
Vol. 80, No. 7, July 2021, pp. 663–673
doi: 10.1093/jnen/nlab052

ORIGINAL ARTICLE

Analyses of DNA Methylation Profiling in the Diagnosis of Intramedullary Astrocytomas

Laetitia Lebrun, MD, Martin Bizet, PhD, Barbara Melendez, PhD, Barbara Alexiou, MPH, Lara Absil, PhD, Claude Van Campenhout, PhD, Nicky D'Haene, MD, PhD, Sandrine Rorive, MD, PhD, François Fuks, PhD, Christine Decaestecker, PhD, and Isabelle Salmon, MD, PhD

Abstract

Intramedullary astrocytomas (IMAs) consist of a heterogeneous group of rare central nervous system (CNS) tumors associated with variable outcomes. A DNA methylation-based classification approach has recently emerged as a powerful tool to further classify CNS tumors. However, no DNA methylation-related studies specifically addressing to IMAs have been performed yet. In the present study, we analyzed 16 IMA samples subjected to morphological and molecular analyses, including DNA methylation profiling. Among the 16 samples, only 3 cases were classified in a reference methylation class (MC) with the recommended calibrated score ($\geq$0.9). The remaining cases were either considered "no-match" cases (calibrated score $<$0.3, n = 7) or were classified with low calibrated scores (ranging from 0.32 to 0.53, n = 6), including inconsistent classification. To obtain a more comprehensive tool for pathologists, we used different unsupervised analyses of DNA methylation profiles, including our data and those from the Heidelberg reference cohort. Even though our cohort included only 16 cases, hypotheses regarding IMA-specific classification were underlined; a potential specific MC of PA_SPINE was identified and high-grade IMAs, probably consisting of H3K27M wild-type IMAs, were mainly associated with ANA_PA MC. These hypotheses strongly suggest that a specific classification for IMAs has to be investigated.

Key Words: 2016 WHO classification, DNA methylation profiling, Glial tumor, Intramedullary astrocytomas, Methylation array, Spinal cord.

INTRODUCTION

Intramedullary astrocytomas (IMAs) are very rare central nervous system (CNS) tumors with an incidence of less than 1% of all CNS tumors (1) and are associated, due to their location, with high morbidity. The 5-year overall survival ranges from 51.5% to 79.5% for low-grade IMAs, while high-grade IMAs have a median survival of 10 months (1–3). While grade 1 and 2 astrocytomas represent specific clinicopathological brain entities in the brain, spinal grade 1 pilocytic astrocytomas and spinal grade 2 diffuse astrocytomas are often grouped together and reported as low-grade IMAs (4, 5). The recently updated 4th edition of the WHO Classification of CNS tumors in 2016 (WHO 2016) drastically changed the histopathological diagnosis by integrating molecular data into daily diagnostic practice to decrease the inherent subjectivity of the morphological diagnosis (6). For the first time, the location of the tumor is part of the diagnosis for a specific class, for instance, linking the midline location to a specific molecular alteration giving rise to the diffuse midline glioma H3K27M-mutant (DMG K27M) diagnosis associated with a poor prognosis (7). It is therefore surprising that no specific classification is available for IMAs since they are classified similarly to brain tumors in their respective chapters. Moreover, recent studies highlighted the impact of CNS regions on the biology of glioma, suggesting that in the same tumor en-

From the Department of Pathology, Erasme University Hospital, Université Libre de Bruxelles (ULB), Brussels, Belgium (LL, BA, LA, CVC, NDH, SR, IS); Laboratory of Cancer Epigenetics, Faculty of Medicine, ULB-Cancer Research Center (U-CRC), Université Libre de Bruxelles (ULB), Brussels, Belgium (MB, FF); Molecular Pathology Research Unit, Department of Pathology, Virgen de la Salud Hospital, Toledo, Spain (BM); Centre Universitaire inter Régional d'expertise en Anatomie Pathologique Hospitalière (CurePath, CHIREC, CHU Tivoli, ULB), Jumet, Belgium (SR); DIAPath, Center for Microscopy and Molecular Imaging, ULB, Gosselies, Belgium (CD, IS) and ; Laboratory of Image Synthesis and Analysis, Brussels School of Engineering/École Polytechnique de Brussels, ULB, Brussels, Belgium (CD, IS).

Send correspondence to: Isabelle Salmon, MD, PhD, Department of Pathology, Erasme University Hospital, Université Libre de Bruxelles (ULB), 808 Route de Lennik, B-1070 Brussels, Belgium; E-mail: isabelle.salmon@erasme.ulb.ac.be.

This study was funded by the "Fonds Erasme" for Medical Research (Brussels, Belgium) and by funding from the "Fonds Yvonne Boël" (Brussels, Belgium).

This work was performed with the support of grants awarded by the "Fonds Erasme" for Medical Research (Brussels, Belgium) and by funding from the "Fonds Yvonne Boël" (Brussels, Belgium). CD is a Senior Research Associate with the F.N.R.S. (Belgian National Fund for Scientific Research). CMMI is supported by the European Regional Development Fund and the Walloon Region (Wallonia-biomed, #411132-957270, project "CMMI-ULB").

The authors declare that they have no competing interests.

Supplementary Data can be found at academic.oup.com/jnen.

tity, distinct clinical and molecular behaviors could be observed according to their location (8).

Only a few studies have focused on the molecular alteration profiles of IMAs. Some studies have shown that the main recurrent molecular alterations are *KIAA1549-BRAF* fusions and *H3F3A* p. K27M (H3K27M) mutations (9, 10), while others did not identify recurrent molecular alterations at all (11). Interestingly, the most frequent molecular alterations found in brain astrocytomas, such as *IDH* mutations, are generally not observed in IMAs or were not classic *IDH1* p. R132H and *IDH2* p. R172H mutations (9, 11–17). In a previous study, we reported that classic molecular alterations observed in brain astrocytomas (*IDH* mutations, *EGFR* alterations, and *TERT* promoter mutations) are very rare in IMAs, with rather poor prognosis associated with *IDH* mutations in low-grade IMAs (15). For high-grade IMAs, the majority of the tumors described in the literature were strongly related to H3K27M mutations (9, 12, 15, 18–22).

Molecular alterations have an impact on epigenetic regulation (22). Indeed, mutations in epigenetic regulator genes encoding enzymes such IDH have been reported to induce DNA hypermethylation, leading to the "glioma CpG island methylator phenotype" (G-CIMP) (23–25). Different genome-wide methylation profiles would be observed in the case of mutations in epigenetic modifiers and lead to the activation of downstream genes (22). DNA methylation is a relatively stable component of the epigenome, specific to the cell but also to the tissue of origin (26, 27); thus, it can be used to establish lineage classification (26, 28). The study of the cancer methylome, which also reflects additional somatic alterations (29), has already been used to identify new-specific methylation clusters among ependymomas (30) and medulloblastomas (31). The German Cancer Research Centre (DKFZ) and Heidelberg University developed a DNA methylation-based classification model for CNS tumors (which we call the "Heidelberg Brain Tumor classifier") (28). This machine learning model was trained on a reference cohort of 2801 samples, regrouping 82 CNS tumor classes (28). This classifier has emerged as a tool to subclassify CNS tumors that may potentially help in the definition of new entities (32, 33).

Artificial intelligence, particularly classifiers obtained by machine (or deep) learning, currently plays an increasing role in pathology (34). However, an inherent problem with such classifiers is that they are designed to generate a result depending on the given input. Very few IMAs (i.e. 6 DMG K27M and 1 pilocytic astrocytoma) were included for the training of the Heidelberg Brain Tumor classifier, as IMA methylation profiles have not been specifically addressed before. Therefore, it remains unclear whether differences exist between the DNA methylation profiles of IMA and those of astrocytomas arising at other CNS regions.

The aim of the present study was to analyze the DNA methylation profiles using supervised (Heidelberg Brain Tumor classifier) and unsupervised methods in a series of 16 IMAs to explore the possibility of exploiting this classification tool for diagnostic purposes in IMAs. We tried to determine whether the particular molecular background of IMAs, or their specific location, would lead to specific methylation profiles of these tumors.

MATERIALS AND METHODS

Patient Cohort

From 21 patients we selected 23 tumor samples diagnosed between 1995 and 2019 from Biobanque Hôpital Erasme-ULB (BERA), BE_NBWB1, Biothèque Wallonie Bruxelles (BWB), BBMRI-ERIC, and Biolibrary of Saint-Luc University Hospital, together with ethical agreements (Brussels, Belgium; ref., P2017/319). The following inclusion criteria were applied to the selected tumors: (i) intramedullary location (i.e. location within the spinal cord), (ii) astrocytoma diagnosis, and (iii) enough tumoral DNA necessary for DNA methylation analysis (at least 250 ng of DNA). The cohort consisted of 9 grade 1 pilocytic, 2 diffuse grade 2, 3 anaplastic grade 3 and 6 grade 4 IMAs. One case was diagnosed as low-grade IMA, as previously described (15). Two patients were included with initial (case 6 and case 8) and recurrent (rec) samples (case 6 rec and 8 rec). In addition, we used 2 grade 2 intramedullary ependymomas as positive validation controls that were expected to be assigned in methylation class (MC) spine ependymoma (EPN_SPINE (28)). Clinical variables such as event-free survival and overall survival were collected as previously described (15).

Pathological Examination

Pathological diagnosis was reviewed by 2 pathologists (L.L. and I.S.) according to the WHO 2016 classification (6), as previously described (15). A detailed morphological analysis was performed for each case, including the presence of Rosenthal fibers, eosinophilic granular bodies, necrosis, the estimation of cellularity (low, moderate, high), atypia (low, moderate, high), vascularization, and descriptions of the tumor architecture (labeled as biphasic, piloid, oligodendroglioma-like, fascicular, or fibrillar). These features were noted as binary variables, if present or not (0/1) (except for cellularity, atypia, vascularization, and tumor architecture). The proliferation index based on KI-67 immunostaining was collected.

Molecular Analyses

Next-Generation Sequencing Assays

Molecular profiles were obtained by using 2 AmpliSeq gene-targeted DNA custom panels ("Clinical Glioma" and "Research Glioma" panels) and a specific *KIAA1549-BRAF* fusion panel, as previously described (15). These 3 panels analyzed a total of 33 genes commonly implicated in gliomas, the 1p and 19q regions and 10 different *KIAA1549-BRAF* fusions described in the COSMIC database (Sanger Institute Catalog of Somatic Mutations in Cancer).

DNA Methylation Profiling

The percentage of tumor cells per sample was evaluated to be greater than 70% for all cases except for cases 2, 3, and 5 (percentage of tumoral cells ranging from 50% to less than 70%).

DNA from formalin-fixed paraffin-embedded (FFPE) tumor tissues was extracted using the QIAamp DNA FFPE Tissue Kit (Qiagen, Manchester, UK) and quantified using a Qubit 2.0 Fluorometer (Thermo Fisher Scientific, Waltham, MA). At least 250 ng of DNA was extracted from FFPE samples. DNA was processed on the IntegraGen platform (Evry, France) using the Illumina Infinium Human Methylation EPIC (850 K) BeadChip array (Illumina, San Diego, CA) following the manufacturer's instructions. Samples were checked for their quality based on the detection p values (suboptimal quality was defined if less than 90% of CpGs were detected with a p value of 0.05). Seven samples presented suboptimal quality control and were excluded from our study (3 grade 1, 2 grade 2, 1 grade 3, and 1 grade 4).

Data Analyses of DNA Methylation Profiling

Supervised Analysis Using the Heidelberg Brain Tumor Classifier

The raw methylation data (IDAT files) were uploaded online (www.molecularneuropathology.org) to obtain MCs using the Heidelberg Brain Tumor classifier, which is a random forest-based MC prediction algorithm (28). Each sample classification was associated with a calibrated score, which provided a confidence index for the MC match. We considered a result as a "match" with a reference MC if a calibrated score of at least 0.9 was obtained, as previously recommended (32, 33, 35). Regarding calibrated scores between 0.3 and 0.9, the interpretation was more problematic and only a diagnostic indication could be obtained. Calibrated scores below 0.3 are generally discarded (35).

Selected Heidelberg Reference Cohort

To set up a more suitable IMA classification, a reference cohort was selected based on Infinium Human Methylation 450 K (450 K) files that are publicly available from the Department of Neuropathology, Heidelberg (28). This select Heidelberg reference cohort comprised only glial tumor MCs consisting of 29 distinct tumoral MCs from intramedullary-midline and supratentorial location (Supplementary File 1). For each of these 29 MCs, approximately 10 samples were selected according to the availability of location data and to the highest tumoral cell purity, leading to a series of 284 samples. Notably, we included 31 cases from intramedullary locations (including 6 DMG K27M and 1 pilocytic astrocytoma) in the selected Heidelberg reference cohort as opposed to 215 that were not. The selected Heidelberg reference cohort also comprised control samples: white matter, pons and reactive tissue MCs (n = 38 samples).

Unsupervised Analysis

This analysis aims to establish the similarities and dissimilarities between the DNA methylation profiles of the IMA cases included in our cohort, as well as between these IMA profiles and the selected Heidelberg reference group.

For the unsupervised analysis, we constructed a meta-cohort combining our DNA methylation data of sufficient quality (based on the detection p value, as described above) with the reference data described above. The resulting data set was preprocessed following the published guidelines (36): CpG probes of low quality (detection p - value threshold of 0.05) or targeting X and Y chromosomes were removed from the analysis. Additionally, probes targeting methylation sites located at common single-nucleotide polymorphisms as well as cross-reactive probes (i.e. targeting several genomic locations) were filtered out based on the extended annotation of McCartney et al (37) (for the 850 K data) or Price et al (38) (for the 450 K data). Beta values were computed using the following formula: Beta-value = M/[U + M] where M and U are the raw "methylated" and "unmethylated" signals, respectively. Beta values were corrected for type I and type II bias using peak-based correction (15). Finally, only probes in common between 450 K and 850 K and kept after preprocessing were selected for further analysis. The standard deviation of the remaining probes was computed across the metacohort, and 15 000 probes showing the larger variation were selected. The data were then normalized and scaled using the "normalize_input" function from the Rtsne package, and principal component analysis (PCA) was performed to extract the first 50 principal components using the R function "prcomp" (with center = TRUE and scale. = FALSE options as the data were already scaled by the normalize_input function). Euclidean distances in the 50-dimensional PCA space were then computed between each possible pair of samples from the meta-cohort. These distances were used to extract the 3 nearest neighbors of each IMA sample from our series (Supplementary File 2) and to perform a hierarchical cluster analysis of the samples (using the "ward.D2" method). Finally, a t-distributed stochastic neighbor embedding (t-SNE) analysis was performed on the 50 principal components using the "Rtsne" function from the Rtsne package. After having set the random seed to 0, we performed t-SNE analysis with pca = FALSE and scale = FALSE (as those steps were already performed outside of the function) and varying the perplexity from 20 to 40 by step 2 (the other parameters were kept as default: theta = 0.5, max_iter = 1000). As t-SNE results can strongly depend on the perplexity value, we finally selected the perplexity value of 22, because it provided coherent results with the neighborhood relations established in the PCA space and the hierarchical clustering analyses.

For all of these analyses, IMA cases from our series were reported by numbers, while cases from the selected Heidelberg reference cohort were assigned to their MC.

RESULTS

Clinical, Pathological, and Molecular Features of the IMA Cohort

Table 1 details the clinical, histopathological, and molecular features of our series. Our cohort consisted of 6 grade 1, 1 low-grade, 2 grade 3, and 5 grade 4 IMA cases.

TABLE 1. Clinical, Histopathological, and Molecular Features of the 14 Intramedullary Astrocytoma (IMA) Patients (16 Samples)

Clinical Features								Histopathological Features	Molecular Alterations	
Cases	Age (Years)	Sex (M/F)	MRI Pattern (C/I)	Location	FU (Months)	Status (A/D)	Recurrence (Y/N)	2016 WHO Grade	Pathological Diagnosis	Pathogenic Mutations	*KIAA1549-BRAF* Fusions Status
1	38	M	C	Lumbar	43	D	Y	4	DMG K27M	*H3F3A K27M, ATRX, PIK3CA*	No fusions
2	15	M	I	Cervical	10	D	ND	4	DMG K27M	*H3F3A K27M, TP53, NF1*	No fusions
3	9	F	ND	Cervico-thoracic	2	A	N	4	DMG K27M	*H3F3A K27M, TP53*	No fusions
4	37	F	I	Thoracic	1	A	N	1	Pilocytic A.	No mutations	*KIAA1549 (15)-BRAF(11)*
5	53	F	I	Thoracic	25	A	N	1	Pilocytic A.	No mutations	*KIAA1549 (15)-BRAF(9)*
6	22	F	I	Thoracic	58	D	Y	3	Anaplastic A.	*ATRX*	No fusions
6rec									Anaplastic A.	*ATRX, PIK3CA*	No fusions
7	27	M	C	Cervical	106	A	N	1	Pilocytic A.	No mutations	No fusions
8	8	M	I	Thoraco-lumbar	136	A	Y	LG	LG A.	No mutations	No fusions
8rec									LG A.	No mutations	No fusions
9	43	F	ND	Thoracic	42	A	Y	3	Anaplastic A.	No mutations	No fusions
10	20	M	C	Cervical	4	A	N	1	Pilocytic A.	No mutations	No fusions
11	5	M	ND	Cervico-thoracic	7	A	N	1	Pilocytic A.	No mutations	*KIAA1549 (15)-BRAF(9)*
12	73	F	ND	Thoraco-lumbar	16	A	N	1	Pilocytic A.	No mutations	No fusions
13	19	M	ND	Thoracic	21	A	Y	4	DMG K27M	*H3F3A p. K27M*	NC
14	70	M	ND	Thoracic	3	A	Y	4	Glioblastoma	*ATRX, TP53, NF1*	No fusions

A: alive; C: well-circumscribed; D: deceased; DMG K27M: diffuse midline glioma, H3K27M mutated; F: female; FU: follow-up; I: infiltrative; LG: low-grade; M: male; N: no; NC: nonconclusive; ND: no data available; rec: recurrent tumor sample; Y: yes.

Of the 16 samples, 13 concerned primary resection samples and 2 second resection samples (cases 6 rec and 8 rec), and for case 9, the sample concerned only a secondary surgery. Among the 14 patients, the median age at diagnosis was 24.5 years, ranging from 5 to 73 years. The male-to-female ratio showed a male predominance (M: F ratio of 1.33). The median follow-up period of the series was 18.5 months, with a range of 1–136 months. Recurrence or disease progression occurred in 6 patients (6/14, 46%) with a median event-free survival of 42.5 months. Three patients (3/14, 21%) died, with a median overall survival of 43 months.

Out of 6 pilocytic grade 1 IMAs, 3 cases harbored *KIAA1549-BRAF* fusions, including 2 *KIAA1549(15)-BRAF(9)* variant fusions and 1 *KIAA1549(15)-BRAF(11)* variant fusion. No driver pathogenic mutations or *KIAA1549-BRAF* fusions were identified among the low-grade IMAs (primary and recurrent samples). One of the 2 anaplastic IMAs (case 6) harbored a pathogenic mutation in *ATRX* (p.Q2042fs) and its recurrence showed an additional mutation in *PIK3CA* (p.W11R) (case 6 rec). Four out of the 5 grade 4 IMAs harbored *H3F3A* p. K27M mutations. Grade 4 H3K27M wild-type (wt) IMA occurred in the context of Lynch syndrome and harbored pathogenic mutations in the *ATRX* (p.F234fs), *TP53* (p.R248Q), and *NF1* (p.R2637Ter) genes.

Supervised Analysis of the DNA Methylation Profiles of IMAs Using the Heidelberg Brain Tumor Classifier

All the IMA samples (n = 16) and 2 control cases (control 1 and control 2) were submitted to the 850 K DNA methylation profiling study. Table 2 details the results provided by the Heidelberg Brain Tumor classifier. As expected, the 2 control cases (control 1 and control 2) were correctly classified as spinal ependymomas (MC EPN_SPINE), both with a calibrated score of 0.99. Three out of the 16 cases matched the reference MC with a calibrated score of at least 0.9. Among these, the Heidelberg Brain Tumor classifier agreed with the pathological diagnosis of DMG K27M for 2 cases (cases 2 and 13). Concerning case 14, the Heidelberg Brain Tumor classifier provided a diagnosis of ANA_PA instead of the pathological diagnosis of *IDH*-wt glioblastoma (WHO grade 4).

Seven cases with calibrated scores less than 0.3 were considered "no-match" cases. The remaining 6 cases had a calibrated score ranging from 0.32 to 0.53, which was too low to consider the MC classification informative with sufficient certainty. Nevertheless, we underlined that case 11, diagnosed as a grade 1 pilocytic IMA was classified as MC family pilocytic astrocytoma and that case 6, diagnosed as anaplastic IMA, was classified as MC ANA_PA. In contrast, cases 6 rec, 7, 10, and 12 (i.e. an anaplastic astrocytoma and 3 pilocytic as-

TABLE 2. Classification of Intramedullary Astrocytomas (IMAs) Using the Heidelberg Brain Tumor Classifier (www.molecularneuropathology.org)

Cases	2016 WHO Grade	Pathological Diagnosis	% of Tumor Cells	Match to Reference MC	Methylation Class (MC)	Calibrated Score
Control 1	2	Ependymoma	>70	**Yes**	**MC EPN_SPINE**	**0.99**
Control 2	2	Ependymoma	>70	**Yes**	**MC EPN_SPINE**	**0.99**
14	4	Glioblastoma	>70	**Yes**	**MC ANA_PA**	**0.96**
2	4	DMG K27M	50–70	**Yes**	**MC DMG_K27M**	**0.99**
13	4	DMG K27M	>70	**Yes**	**MC DMG_K27M**	**0.99**
10	1	Pilocytic A.	>70	No	MC family plexus tumor	0.32
11	1	Pilocytic A.	>70	No	MC family pilocytic astrocytoma	0.35
12	1	Pilocytic A.	>70	No	MC family GBM IDH-wt	0.35
6	3	Anaplastic A.	>70	No	MC ANA_PA	0.35
6 rec	3	Anaplastic A.	>70	No	MC family plexus tumor	0.41
7	1	Pilocytic A.	>70	No	MC EPN_SPINE	0.53
1	4	DMG K27M	>70	No	NA	<0.3
3	4	DMG K27M	50–70	No	NA	<0.3
4	1	Pilocytic A.	>70	No	NA	<0.3
5	1	Pilocytic A.	50–70	No	NA	<0.3
8	LG	LG A.	>70	No	NA	<0.3
8 rec	LG	LG A.	>70	No	NA	<0.3
9	3	Anaplastic A.	>70	No	NA	<0.3

A: astrocytoma; ANA_PA: anaplastic pilocytic astrocytoma; DMG H3K27M: diffuse midline glioma, H3K27M mutated; EPN_SPINE: spine ependymoma; GBM: glioblastoma; LG: low-grade; MC: methylation class; NA: not applicable.
Cases in bold were classified with a calibrated score ≥0.9.

trocytomas, respectively) presented discordance between histology/molecular and methylation. For cases 6 rec and 10, the Heidelberg Brain Tumor classifier provided a diagnosis of plexus tumor. Case 6 rec died after a follow-up of 58 months. The follow-up of case 10 (4 months) was too short to be taken into consideration. For case 12, while the Heidelberg Brain Tumor classifier provided a diagnosis of *IDH*-wt GBM, this case did not experience recurrence and was still alive after a follow-up of 16 months. For case 7, diagnosed as an ependymoma by the Heidelberg Brain Tumor classifier, no recurrences or death was noted during the follow-up of 106 months.

Unsupervised Analysis of the DNA Methylation Profiles of IMAs

To characterize the Heidelberg Brain Tumor classifier results and eventually to identify specific clusters for IMAs, we decided to perform different unsupervised analyses with different tools. For this purpose, we combined the selected Heidelberg reference cohort described in Supplementary File 1 (n = 284, including 38 control samples) and our IMA cases (n = 16).

We first performed a PCA to extract the 50 principal components in order to ensure a sufficient percentage of explained variance (79.42%). In this data space, we determined the 3 nearest-neighbor cases of each IMA profile (Supplementary File 2) and applied hierarchical clustering (Fig. 1). t-SNE analysis (Fig. 2) was used to identify and visualize potential clusters of DNA methylation profiles. The first nearest neighbors of the 16 IMAs tested consisted of 11 cases from our IMA series and 5 cases from the selected Heidelberg reference cohort (Supplementary File 2). All these nearest-neighbor cases of our cohort were located in intramedullary locations, except for case 11, whose nearest neighbor was located in the posterior fossa.

As detailed below, among the 29 Heidelberg reference tumoral MCs represented in our hierarchical clustering and t-SNE models, our IMA cases were fitted with 2 MCs: DMG_K27M (4 cases) and ANA_PA (2 cases), whereas 5 cases (4, 5, 10, 11, and 12) were organized in a specific IMA cluster that we called PA_SPINE. Three cases (cases 7, 9, 8-8 rec) were considered isolated cases, including 2 cases (cases 7 and 9) very close to the reference MC EPN_SPINE.

PA_SPINE Cluster

Cases 10, 11, and 12 (pilocytic IMAs) had a grade 1 pilocytic astrocytoma as their nearest neighbor. These results were confirmed using hierarchical clustering and t-SNE and contrast with the diagnostic discordances shown for cases 10 and 12 by the Heidelberg Brain Tumor classifier (as detailed above). Interestingly, the nearest neighbors of cases 4 and 5 (also pilocytic IMAs) were case 11 and case 12, respectively. These results agreed with the specific cluster of cases 4, 5, 10, 11, and 12 proposed by the hierarchical clustering and t-SNE analyses, referred to hereafter as "PA_SPINE" cluster.

The 5 grade 1 pilocytic IMAs constituting the PA_SPINE cluster presented PA morphology with a biphasic (n = 3), piloid (n = 4), or oligodendroglioma-like pattern (n = 1) with Rosenthal fibers (n = 5) and eosinophilic granular bodies (n = 3). Cellularity ranged from moderate to high with few to moderate cellular atypia. Vessel hyalinization was pre-

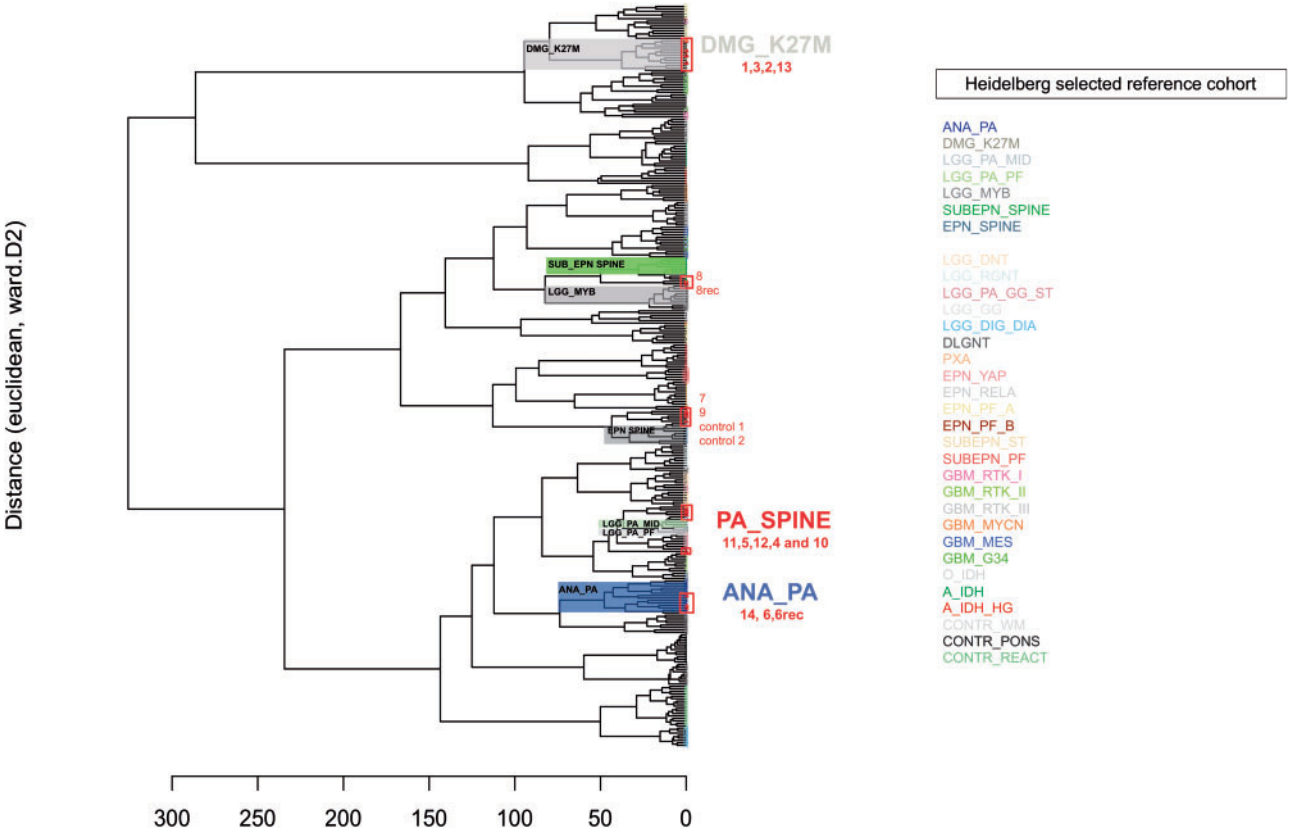

FIGURE 1. Hierarchical clustering was carried out on the first 50 principal components extracted from the DNA methylation profiles grouping our IMA cases (illustrated in red, n = 16) and the selected Heidelberg reference cohort (n = 284). From the Heidelberg reference cohort, 7 clusters were reported: MC SUB_EPN (green), MC LGG_PA_MID (light green), MC EPN_SPINE (dark gray), MC DMG_K27M and LGG_MYB (gray), MC LGG_PA_PF (pink), and MC ANA_PA (blue). A_IDH: *IDH*-mutated astrocytoma; ANA_PA: anaplastic pilocytic astrocytoma; DLGNT: diffuse leptomeningeal glioneuronal tumor; DMG K27M: diffuse midline glioma, H3K27M-mutated; DNT: dysembryoplastic neuroepithelial tumor; EPN_PF: posterior fossa ependymoma; EPN_RELA: ependymoma RELA fusion; EPN_SPINE: spine ependymoma; EPN_YAP: ependymoma YAP fusion; GBM MES MYCN RTK I II III: glioblastoma subclass mesenchymal, MYCN, RTK I, II, III; GBM MID: midline glioblastoma; HG: high-grade; LGG_DIG_DIA: low-grade desmoplastic infantile astrocytoma/ganglioglioma; LGG_GG: low-grade glioma ganglioglioma; LGG_GG_PA_ST: supratentorial low-grade ganglioglioma pilocytic astrocytoma; LGG_MYB: low-grade glioma MYB-altered; MC: methylation class; O_IDH: *IDH*-mutated oligodendroglioma; PA_MID: midline pilocytic astrocytoma; PA_PF: posterior fossa pilocytic astrocytoma; PXA: pleomorphic xanthoastrocytoma; RGNT: rosette-forming glioneuronal tumor; SUB_EPN SPINE: spine subependymoma; SUB_EPN ST: supratentorial subependymoma; SUB_EPN_PF: posterior fossa subependymoma.

sent in 3 cases. The KI-67 proliferation index ranged from less than 2–5%. While harboring PA morphology, a heterogeneous molecular profile according to *KIAA1549-BRAF* fusions was noted. Only 3 out of the 5 cases harbored *KIAA1549-BRAF* fusions (cases 4, 5, and 11, see Table 3). The *KIAA1549-BRAF* fusion was not detected in cases 10 and 12, while it was detected in their nearest neighbors (cases 11 and 4, see Supplementary File 2).

ANA_PA Cluster

Case 14, assigned by the Heidelberg Brain Tumor classifier to MC ANA_PA with a calibrated score of at least 0.9, had as its first nearest neighbor a case from our IMA series (case 6), which had a pathological diagnosis of anaplastic IMA. We observed that the 3 nearest neighbors of case 6 consisted of its second resection (case 6 rec) and 2 reference MC ANA_PA cases (Supplementary File 2). These neighborhood relations were also confirmed by hierarchical clustering and t-SNE, which highlighted that case 14 closely clustered with case 6 and reference MC ANA_PA cases. Interestingly, the closest case of case 6 rec was a DMG K27M case from our IMA series (Supplementary File 2). Cases 6-6 rec and 14, 1 anaplastic IMA and 1 glioblastoma associated with Lynch syndrome, respectively, were included in the ANA_PA cluster. All of these high-grade IMAs showed no specific morphological characteristics. Necrosis was noted for case 14.

In addition, case 6-6 rec harbored a more fasciculate pattern than case 14, few Rosenthal fibers, and eosinophilic granular bodies (Fig. 3A). In contrast, case 14 harbored marked cellular atypia with numerous multinucleate cells without piloid, biphasic or oligodendroglioma-like patterns, Rosenthal fibers or eosinophilic granular bodies (Fig. 3B). Despite these morphological differences, these 2 cases harbored a patho-

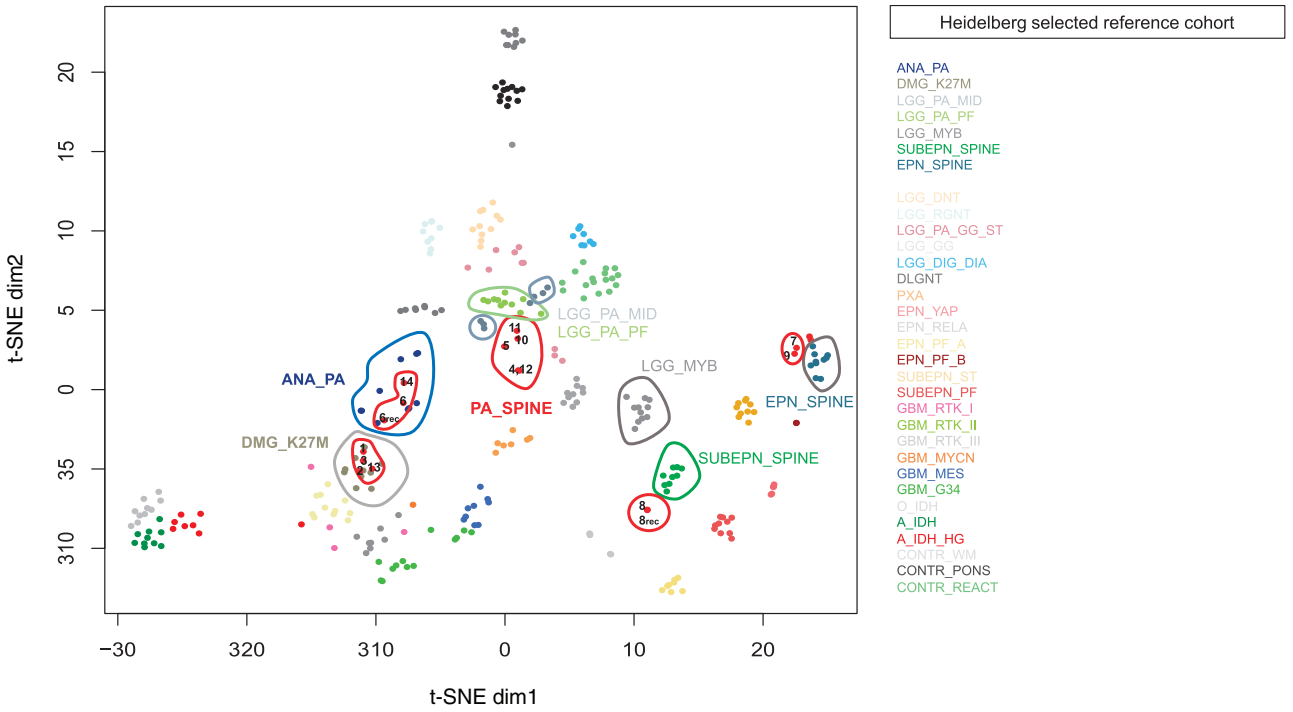

FIGURE 2. t-distributed stochastic neighbor embedding (t-SNE) plot: 2-dimensional representation of our IMA cases (illustrated in red, n = 16) and the selected Heidelberg reference cohort (n = 284). From the Heidelberg reference cohort, 7 clusters were reported: MC SUB_EPN (green), MC LGG_PA_MID (light green), MC EPN_SPINE (dark gray), MC DMG_K27M and LGG_MYB (gray), MC LGG_PA_PF (pink), and MC ANA_PA (blue). A_IDH: *IDH*-mutated astrocytoma; ANA_PA: anaplastic pilocytic astrocytoma; DLGNT: diffuse leptomeningeal glioneuronal tumor; DMG K27M: diffuse midline glioma, H3K27M-mutated; DNT: dysembryoplastic neuroepithelial tumor; EPN_PF: posterior fossa ependymoma; EPN_RELA: ependymoma RELA fusion; EPN_SPINE: spine ependymoma; EPN_YAP: ependymoma YAP fusion; GBM MES MYCN RTK I II III: glioblastoma subclass mesenchymal, MYCN, RTK I, II, III; GBM_MID: midline glioblastoma; HG: high-grade; LGG_DIG_DIA: low-grade desmoplastic infantile astrocytoma/ganglioglioma; LGG_GG: low-grade glioma ganglioglioma; LGG_GG_PA_ST: supratentorial low-grade ganglioglioma pilocytic astrocytoma; LGG_MYB: low-grade glioma MYB-altered; MC: methylation class; O_IDH, *IDH*-mutated oligodendroglioma; PA_MID: midline pilocytic astrocytoma; PA_PF: posterior fossa pilocytic astrocytoma; PXA: pleomorphic xanthoastrocytoma; RGNT: rosette-forming glioneuronal tumor; SUB_EPN SPINE: spine subependymoma; SUB_EPN ST: supratentorial subependymoma; SUB_EPN_PF: posterior fossa subependymoma.

genic *ATRX* mutation, a common molecular feature of MC ANA_PA (Table 3).

DMG_K27M Cluster

As illustrated in Figures 1 and 2, H3K27M-mutated IMAs were included in the DMG K27M cluster using hierarchical clustering and t-SNE. The nearest-neighborhood relations reported in Supplementary File 2, as well as hierarchical clustering and t-SNE visualization, clearly confirmed the MC DMG_K27M assigned by the Heidelberg Brain Tumor classifier (with a calibrated score of at least 0.9) to cases 2 and 13, in agreement with the pathological diagnosis of DMG K27M. For cases 1 and 3, we also observed that their nearest neighbors were part of the reference MC DMG_K27M, also highlighted by hierarchical clustering and t-SNE. These 4 cases with DNA methylation profiles close to that of MC DMG_K27M exhibited high-grade morphological features with necrosis, moderate to high cellularity, moderate to strong atypia and microvascular proliferation. Two cases harbored focally an oligodendroglioma-like pattern (cases 1 and 13), and one other (case 3) harbored a piloid pattern. The KI-67 proliferation index was evaluated to 10%. All of these cases harbored a *H3F3A* p. K27M mutation.

Isolated Cases

Case 7, diagnosed as a grade 1 pilocytic IMA, had 2 of its 3 nearest neighbors from reference MC EPN_SPINE. This is concordant with MC EPN_SPINE being assigned to this case by the Heidelberg Brain Tumor classifier (with a calibrated score of 0.53). Hierarchical clustering and t-SNE confirmed proximity between case 7 and the reference MC EPN_SPINE cases, also suggesting the diagnosis of ependymoma for case 7. This case harbored a fascicular architecture and telangiectatic vascularization without ependymal differentiation (no perivascular pseudorosettes and no ependymal rosettes). No Rosenthal fibers or eosinophilic granular bodies were observed. Facing this challenging morphological case, EMA immunohistochemistry was carried out, revealing focal dot-like staining (Fig. 4A–C).

TABLE 3. Morphological and Molecular Features of Intramedullary Astrocytomas (IMAs) Included in the 3 DNA Methylation Clusters (DMG K27M, ANA_PA, and PA_SPINE) and Isolated Cases (cases 7, 9, 8, and 8 rec).

Cases	Cluster	2016 WHO Grade	Pathological Diagnosis	Pathogenic Mutations	*KIAA1549-BRAF*	Pattern	Rosenthal Fibers	EGB	Necrosis	Cellularity	Atypia	KI-67	Vascularization
1	DMG_K27M	4	DMG K27M	*H3F3A pK27M, ATRX, PIK3CA*	No fusions	O/FA	0	0	1	***	***	10%	microvascular proliferation
2		4	DMG K27M	*H3F3A p. K27M, TP53, NF1*	No fusions	/	0	0	1	***	***	10%	microvascular proliferation
3		4	DMG K27M	*H3F3A p. K27M, TP53*	No fusions	P	0	0	1	**	**	10%	microvascular proliferation
13		4	DMG K27M	*H3F3A p. K27M*	NC	O	0	0	1	**	**	10%	hyalinized, microvascular proliferation
4	PA_SPINE	1	Pilocytic Astrocytoma	No mutations	*KIAA1549(15)-BRAF(11)*	B/P/F	1	1	0	**	*	<2%	hyalinized
5		1	Pilocytic Astrocytoma	No mutations	*KIAA1549(15)-BRAF(9)*	P	1	1	0	***	**	<2%	/
10		1	Pilocytic Astrocytoma	No mutations	No fusions	B/P	1	1	0	**	**	2–5%	hyalinized
11		1	Pilocytic Astrocytoma	No mutations	*KIAA1549(15)-BRAF(9)*	B/P/O	1	0	0	**	*	3%	/
12		1	Pilocytic Astrocytoma	No mutations	No fusions	P	1	0	0	**	*	<2%	hyalinized
6	ANA_PA	3	Anaplastic Astrocytoma	*ATRX*	No fusions	FA	1	1	0	***	***	2–5%	telangiectatic, hyalinized, microvascular proliferation
6 rec[a]		3	Anaplastic Astrocytoma	*ATRX, PIK3CA*	No fusions	FA	0	0	0	***	***	>5%	microvascular proliferation
14		4	Glioblastoma	*ATRX, TP53, NF1*	No fusions	/	0	0	1	***	***	10–15%	microvascular proliferation
8	Isolated cases	LG	LG Astrocytoma	No mutations	No fusions	FA	0	0	0	***	**	<1%	hyalinized, microvascular proliferation
8 rec		LG	LG Astrocytoma	No mutations	No fusions	FA	0	0	0	***	**	<2%	hyalinized, microvascular proliferation
7	Isolated cases	1	Pilocytic Astrocytoma	No mutations	No fusions	FA	0	0	0	**	**	<1%	telangiectatic
9[a]		3	Anaplastic Astrocytoma	No mutations	No fusions	F	0	0	0	***	***	ND	hyalinized

[a]Post RT context, ND: no data available, NC: nonconclusive. ***: high; **: moderate; *: low; 0: absent/1: present; ANA_PA: anaplastic pilocytic astrocytoma; B: biphasic; DMG H3K27M: diffuse midline glioma, H3K27M mutated; EGB: eosinophilic granular bodies; F: fibrillar; FA: fascicular; O: oligodendroglioma-like; P: piloid; PA: pilocytic astrocytoma.

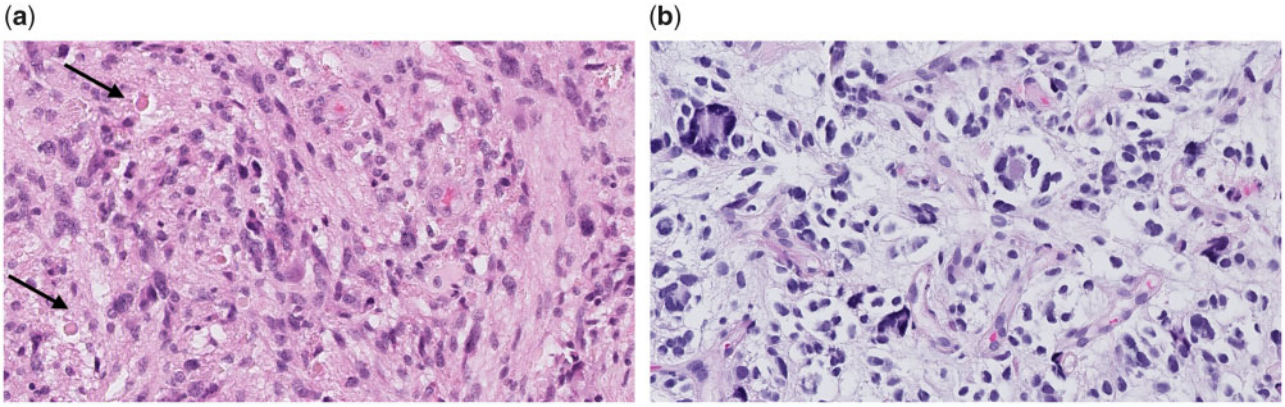

FIGURE 3. Histopathological features of (**A**) Case 6 and (**B**) Case 14 (H&E staining, ×200). The black arrow targeted the eosinophilic granular bodies.

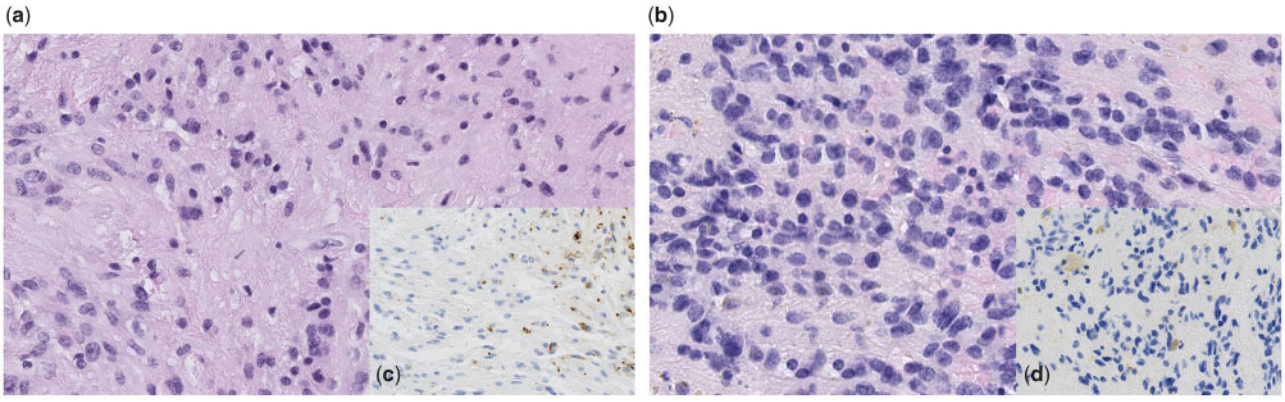

FIGURE 4. Histopathological features of (**A**) Case 7 (hematoxylin and eosin staining [H&E], ×200) and (**B**) Case 9 (H&E, ×200) and EMA immunohistochemistry for Case 7 (**C**) and Case 9 (**D**).

Regarding case 9 (an anaplastic IMA closely located to case 7), neither neighbor relations, hierarchical clustering, nor t-SNE helped us to classify it. For this case, we observed a typical high-grade astrocytoma morphology (Table 3). No EMA antigenicity was noted (Fig. 4B–D). Both of these cases harbored no molecular alterations (among those tested) and remain difficult to classify. Finally, cases 8 and 8 rec were their respective first nearest neighbors, but no other interesting information was provided by the other neighbor relations, hierarchical clustering or t-SNE.

DISCUSSION

Following the 2016 WHO guidelines, CNS tumor classification was applied using the same criteria for supratentorial, infratentorial, posterior fossa, and intramedullary gliomas, regardless of location. Progress is still required, especially for rare and poorly understood entities (29). The present study suggests that IMAs need specific diagnostic criteria development.

In the CNS, location is clearly associated with specific types of tumors. Indeed, glial tumors, such as pilocytic astrocytoma, often comprise distinct clinical and molecular features reflecting specific signatures from their respective brain regions (8). It was also suggested that *IDH*-mutated and *IDH*-wild-type diffuse gliomas, sharing different preferential locations, are derived from different precursor cells (6). The tumor microenvironment plays a key role in gliomagenesis and in the malignant behavior of gliomas regarding cell motility and invasion (8, 39–41).

The Heidelberg Brain Tumor classifier based on DNA methylation profiles has been shown to be a powerful tool even for challenging CNS tumors (42, 43). Among the 1155 prospective samples tested, Capper et al (35) reported 88% of classified cases (with calibrated scores of at least 0.9). In the same way, Jaunmuktane et al (32) reported a rate of 56% of CNS tumors matching a known MC (with calibrated scores of at least 0.84), while Lucas et al (44) reported 40% of match cases (with calibrated scores of at least 0.9) in a cohort of low-grade neuroepithelial tumors. Moreover, Karimi et al (43) reported that 84% of the cases tested with this tool had a clinically significant change in the histopathological diagnosis, with 15% of all those cases associated with a change in clinical decision-making for the patient. DNA methylation-based classification could therefore provide an additional layer helping in the reproducibility and standardization of CNS tumor diag-

nosis (29). However, machine learning classifiers are generally associated with some limitations. First, the performance and scope of application are highly dependent on the data used for training the classifier, with a significant impact of class imbalance (45, 46). Another limitation of the Heidelberg Brain Tumor classifier relates to the confidence index designed as a calibrated score. A threshold of at least 0.9 was determined to optimize both the sensitivity and specificity associated with an MC assigned to a sample (35). Between 0.3 and 0.9, no general recommendation is made, making it difficult to interpret such results. In our study, only 3 out of the 16 IMA cases were robustly classified (calibrated scores of at least 0.9) in a reference MC. These poor results might be due to the low number of IMA cases used to train the Heidelberg Brain Tumor classifier, that is, 1 pilocytic astrocytoma and 6 DMG K27M. In a similar way, a recent study highlighted the limitations of this classifier for other rare tumors, such as NTRK-fused gliomas, with only 2 out of 18 cases matching with high confidence to reference MCs (47). Therefore, more accurate data collection is critically needed to improve such a tool.

Among the 6 IMA cases classified with a calibrated score ranging from 0.3 to less than 0.9, 4 cases presented discordance between histology/molecular and methylation. These data confirm that considering an MC with a calibrated score lower than 0.9 can be prone to error and that the integration of the DNA methylation diagnosis with all clinical data, including morphological diagnosis, remains crucial.

In view of the above limitations, we decided to use different unsupervised analysis techniques. Capper et al (35) also used an unsupervised analysis to explain the "no-match" decisions obtained with their prospective cohort. Interestingly, using t-SNE, the DNA methylation profiles of these cases appeared in the periphery of, or totally separated from, the reference MCs and often clustered with other "no-match" cases. Capper et al concluded that these "no-match" cases did correspond to new entities that were not yet included in the training set of their classifier. In another recent study, unsupervised methods evidenced DNA methylation profiles of infratentorial *IDH*-mutant astrocytomas (located in the brainstem and cerebellum) that differed from those of supratentorial *IDH*-mutants, whereas the Heidelberg Brain Tumor classifier allocated all of these tumors to MC A_IDH (48).

In the present study, we identified a specific cluster of pilocytic IMAs, supported by both unsupervised analysis of DNA methylation profiles and morphological examination. These cases did not cluster with reference MC PA cases (MC PA_PF, MC PA_MID, or MC PA_ST). All these data motivated us to define a specific "MC PA_SPINE" that has to be validated with more cases.

Interestingly, the remaining low-grade IMA cases (one pilocytic IMA and one low-grade IMA, primary and recurrent samples) appeared as isolated cases in terms of DNA methylation profiles. One of them was closely located to the reference MC EPN_SPINE, and despite not harboring ependymal morphology, it was associated with EMA antigenicity. This raises the question about the cooccurrence of astrocytic and ependymal differentiation. Some mixed ependymomas and astrocytomas have already been described in literature (49). Nevertheless, it is sometimes challenging to make such differential diagnosis in medullary locations especially for tanycytic ependymomas, which can be misdiagnosed as astrocytomas (50). Therefore, this pilocytic IMA could be an ependymoma that has been misdiagnosed as a pilocytic astrocytoma based on microscopic features.

Nearly all H3K27M-wt high-grade IMA cases were clustered with the reference MC ANA_PA. This result agrees with the *ATRX* mutation harbored by all H3K27M-wt high-grade IMAs, that is, one of the molecular hallmarks of ANA_PA (51). This fact could raise the question about the specificities of anaplastic evolution, uncommon in spine location, as it is described in only 7% of "pediatric-type" diffuse gliomas (52). This outcome could suggest a unique biological behavior of IMAs and raise the question of the existence of secondary anaplastic astrocytomas and glioblastomas in the spinal cord.

In addition to specific clinical and molecular features (15), all these results are in favor of epigenetic specificities of IMAs compared to those from other locations. These epigenetic specificities could be explained by specific molecular alterations in epigenetic regulators. As *IDH* mutations for brain astrocytomas, other epigenetic regulators may be implicated in IMAs. Moreover, as DNA methylation profiling is clearly influenced by markers from the microenvironment, the specific composition of this latter could be another explanation of the DNA methylation specificity of IMAs.

Finally, we observed a good concordance level (73%, 8/11, data not shown) in terms of a morphological diagnosis between our "no-match" cases or cases with an inconsistent MC (with calibrated scores less than 0.9) and their nearest neighbors in terms of DNA methylation profiles.

Conclusion

DNA methylation classification has emerged as a powerful machine learning approach for clinical decision-making and in the improvement of the biological understanding of CNS tumors. To more efficiently train machine learning models, the enrichment of DNA methylation databases by infrequent CNS neoplasms such IMAs is crucially needed. Even though our cohort included only 16 cases (without grade 2 diffuse IMAs), hypotheses regarding IMA-specific classification were underlined; a potential specific MC of PA_SPINE was identified and high-grade IMAs probably consisting of H3K27M-wt IMAs were mainly associated with ANA_PA. These hypotheses strongly suggest that a specific classification for IMAs has to be developed.

ACKNOWLEDGMENTS

The authors thank Corentin Martens, Dominique Penninck, and Ghita Tagmouti for their logistical help.

REFERENCES

1. Abd-El-Barr MM, Huang KT, Chi JH. Infiltrating spinal cord astrocytomas: Epidemiology, diagnosis, treatments and future directions. J Clin Neurosci 2016;29:15–20
2. Hamilton KR, Lee SS, Urquhart JC, et al.. A systematic review of outcome in intramedullary ependymoma and astrocytoma. J Clin Neurosci 2019;63:168–75
3. Ostrom QT, Cioffi G, Gittleman H, et al.. CBTRUS statistical report: Primary brain and other central nervous system tumors diagnosed in the United States in 2012–2016. Neuro Oncol 2019;21:v1–100

4. Seki T, Hida K, Yano S, et al.. Clinical factors for prognosis and treatment guidance of spinal cord astrocytoma. Asian Spine J 2016;10:748
5. Khalid S, Kelly R, Carlton A, et al. Adult intradural intramedullary astrocytomas: A multicenter analysis. J Spine Surg 2019;5:19–30
6. Louis DN, Louis, DN Ohgaki, H, et al.. WHO classification of tumours of the central nervous system. Revised 4th. In: Louis DN, Ohgaki H, Wiestler OD, Cavenee WK, eds. *WHO classification of tumours of the central nervous system*. Lyon: International Agency for Research on Cancer 2016:408
7. Sturm D, Witt H, Hovestadt V, et al.. Hotspot mutations in H3F3A and IDH1 define distinct epigenetic and biological subgroups of glioblastoma. Cancer Cell 2012;22:425–37
8. Chen Y-H, Gutmann DH. The molecular and cell biology of pediatric low-grade gliomas. Oncogene 2014;33:2019–26
9. Shankar GM, Lelic N, Gill CM, et al.. BRAF alteration status and the histone H3F3A gene K27M mutation segregate spinal cord astrocytoma histology. Acta Neuropathol 2016;131:147–50
10. Grob S, Nobre L, Campbell K, et al.. Clinical and molecular characterization of a multi-institutional cohort of pediatric spinal cord low-grade gliomas. Neurooncol Adv 2020;2:vdaa103
11. Zhang M, Iyer RR, Azad TD, et al.. Genomic landscape of intramedullary spinal cord gliomas. Sci Rep 2019;9:18722
12. Chai R-C, Zhang Y-W, Liu Y-Q, et al.. The molecular characteristics of spinal cord gliomas with or without H3 K27M mutation. Acta Neuropathol Commun 2020;8:40
13. Deng L, Xiong P, Luo Y, et al.. Association between IDH1/2 mutations and brain glioma grade. Oncol Lett 2018;16:5405–9
14. Ellezam B, Theeler BJ, Walbert T, et al.. Low rate of R132H IDH1 mutation in infratentorial and spinal cord grade II and III diffuse gliomas. Acta Neuropathol 2012;124:449–51
15. Lebrun L, Meléndez B, Blanchard O, et al.. Clinical, radiological and molecular characterization of intramedullary astrocytomas. Acta Neuropathol Commun 2020;8:128
16. Takai K, Tanaka S, Sota T, et al.. Spinal cord astrocytoma with isocitrate dehydrogenase 1 gene mutation. World Neurosurg 2017;108:991.e13–16
17. Cheng X, Lou S, Huang S, et al.. Primary spinal cord glioblastoma multiforme: A retrospective study of patients at a single institution. World Neurosurg 2017;106:113–9
18. Alvi MA, Ida CM, Paolini MA, et al.. Spinal cord high-grade infiltrating gliomas in adults: Clinico-pathological and molecular evaluation. Mod Pathol 2019;32:1236–43
19. Sloan EA, Cooney T, Oberheim Bush NA, et al.. Recurrent non-canonical histone H3 mutations in spinal cord diffuse gliomas. Acta Neuropathol 2019;138:877–81
20. Yi S, Choi S, Shin DA, et al.. Impact of H3.3 K27M mutation on prognosis and survival of grade IV spinal cord glioma on the basis of new 2016 World Health Organization Classification of the Central Nervous System. Neurosurgery 2019;84:1072–81
21. Zhang Y-W, Chai R-C, Cao R, et al.. Clinicopathological characteristics and survival of spinal cord astrocytomas. Cancer Med 2020;9:6996–7006
22. Lee C-J, Ahn H, Jeong D, et al.. Impact of mutations in DNA methylation modification genes on genome-wide methylation landscapes and downstream gene activations in pan-cancer. BMC Med Genomics 2020;13:27
23. Bai H, Harmancı AS, Erson-Omay EZ, et al.. Integrated genomic characterization of IDH1-mutant glioma malignant progression. Nat Genet 2016;48:59–66
24. Dang L, Yen K, Attar EC. IDH mutations in cancer and progress toward development of targeted therapeutics. Ann Oncol 2016;27:599–608
25. Huang J, Yu J, Tu L, et al.. Isocitrate dehydrogenase mutations in glioma: From basic discovery to therapeutics development. Front Oncol 2019;9:506
26. Kim M, Costello J. DNA methylation: An epigenetic mark of cellular memory. Exp Mol Med 2017;49:e322
27. Brena RM, Huang TH-M, Plass C. Toward a human epigenome. Nat Genet 2006;38:1359–60
28. Capper D, Jones DTW, Sill M, et al.. DNA methylation-based classification of central nervous system tumours. Nature 2018;555:469–74
29. Hegi ME, Kleihues P, Wen PY, et al.. Toward methylation-based classification of central nervous system tumors. Neuro Oncol 2018;20:579–81
30. Pajtler KW, Witt H, Sill M, et al.. Molecular classification of ependymal tumors across all cns compartments, histopathological grades, and age groups. Cancer Cell 2015;27:728–43
31. Schwalbe EC, Williamson D, Lindsey JC, et al.. DNA methylation profiling of medulloblastoma allows robust sub-classification and improved outcome prediction using formalin-fixed biopsies. Acta Neuropathol 2013;125:359–71
32. Jaunmuktane Z, Capper D, Jones DTW, et al.. Methylation array profiling of adult brain tumours: Diagnostic outcomes in a large, single centre. Acta Neuropathol Commun 2019;7:24
33. Priesterbach-Ackley LP, Boldt HB, Petersen JK, et al.. Brain tumour diagnostics using a DNA methylation-based classifier as a diagnostic support tool. Neuropathol Appl Neurobiol 2020;46:478–92
34. Cohen S. Artificial intelligence and deep learning in pathology. In: Stanley Cohen, eds. Artificial Intelligence and Deep Learning in Pathology. Amsterdam: Elsevier 2021:1–12. Available from: https://linkinghub.elsevier.com/retrieve/pii/B9780323675383010010
35. Capper D, Stichel D, Sahm F, et al.. Practical implementation of DNA methylation and copy-number-based CNS tumor diagnostics: The Heidelberg experience. Acta Neuropathol 2018;136:181–210
36. Dedeurwaerder S, Defrance M, Bizet M, et al.. A comprehensive overview of Infinium HumanMethylation450 data processing. Brief Bioinform 2014;15:929–41
37. McCartney DL, Walker RM, Morris SW, et al.. Identification of polymorphic and off-target probe binding sites on the Illumina Infinium MethylationEPIC BeadChip. Genom Data 2016;9:22–4
38. Price ME, Cotton AM, Lam LL, et al.. Additional annotation enhances potential for biologically-relevant analysis of the Illumina Infinium HumanMethylation450 BeadChip array. Epigenetics Chromatin 2013;6:4
39. Maria BL, Gupta N, Gilg AG, et al.. Targeting hyaluronan interactions in spinal cord astrocytomas and diffuse pontine gliomas. J Child Neurol 2008;23:1214–20
40. Maris C, Rorive S, Sandras F, et al.. Tenascin-C expression relates to clinicopathological features in pilocytic and diffuse astrocytomas. Neuropathol Appl Neurobiol 2008;34:316–29
41. Rauschenbach L. Spinal cord tumor microenvironment. In: Birbrair A, ed. Tumor Microenvironments in Organs. Springer International Publishing 2020:97–109 [cited 2020 March 10]. Available from: http://link.springer.com/10.1007/978-3-030-36214-0_8
42. Perez E, Capper D. Invited review: DNA methylation-based classification of paediatric brain tumours. Neuropathol Appl Neurobiol 2020;46:28–47
43. Karimi S, Zuccato JA, Mamatjan Y, et al.. The central nervous system tumor methylation classifier changes neuro-oncology practice for challenging brain tumor diagnoses and directly impacts patient care. Clin Epigenet 2019;11:185
44. Lucas C-HG, Gupta R, Doo P, et al.. Comprehensive analysis of diverse low-grade neuroepithelial tumors with FGFR1 alterations reveals a distinct molecular signature of rosette-forming glioneuronal tumor. Acta Neuropathol Commun 2020;8:151
45. Kumar R, Liu APY, Orr BA, et al.. Advances in the classification of pediatric brain tumors through DNA methylation profiling: From research tool to frontline diagnostic: Classification of Pediatric Brain Tumors. Cancer 2018;124:4168–80
46. Therrien R, Doyle S. Role of training data variability on classifier performance and generalizability. In: Medical Imaging 2018: Digital Pathology. International Society for Optics and Photonics. cited 2020 November 26.
47. Torre M, Vasudevaraja V, Serrano J, et al.. Molecular and clinicopathologic features of gliomas harboring NTRK fusions. Acta Neuropathol Commun 2020;8:107
48. Banan R, Stichel D, Bleck A, et al.. Infratentorial IDH-mutant astrocytoma is a distinct subtype. Acta Neuropathol 2020;140:569–81
49. Weinstein GM, Arkun K, Kryzanski J, et al.. Spinal intradural, extramedullary ependymoma with astrocytoma component: A case report and review of the literature. Case Rep Pathol 2016;2016:3534791–5
50. Neumann JE, Spohn M, Obrecht D, et al.. Molecular characterization of histopathological ependymoma variants. Acta Neuropathol 2020;139:305–18
51. Reinhardt A, Stichel D, Schrimpf D, et al.. Anaplastic astrocytoma with piloid features, a novel molecular class of IDH wildtype glioma with recurrent MAPK pathway, CDKN2A/B and ATRX alterations. Acta Neuropathol 2018;136:273–91
52. Jones C, Perryman L, Hargrave D. Paediatric and adult malignant glioma: Close relatives or distant cousins? Nat Rev Clin Oncol 2012;9:400–13